

Why some Iron-based superconductors are nodal while others are nodeless

Ronny Thomale,¹ Christian Platt,² Werner Hanke,² and B. Andrei Bernevig¹

¹*Department of Physics, Princeton University, Princeton, NJ 08544*

²*Institute for Theoretical Physics and Astrophysics,
University of Würzburg, Am Hubland, D 97074 Würzburg*

(Dated: February 23, 2024)

The symmetry of the order parameter in iron-based superconductors, especially the presence or absence of nodes, is still a question of debate. While contradictory experiments can be explained by appropriately tuned theories of nodeless superconductivity in the iron-arsenide compounds, for LaOFeP all experiments clearly point to a nodal order parameter. We put forward a scenario that naturally explains the difference between the order-parameter character in these two sets of compounds, and use functional renormalization group (fRG) techniques to analyze it in detail. Our results show that, due to the orbital content of the electron and hole bands, nodal superconductivity on the electron pockets (hole pocket gaps are always nodeless) can naturally appear when the third hole pocket which lies at wavevector (π, π) in the unfolded Brillouin zone is absent, as is the case in LaOFeP. When present, the third hole pocket has overwhelming d_{xy} orbital character, and the intra-orbital interaction with the d_{xy} dominated part of the electron Fermi surface is enough to drive the superconductivity nodeless (of s_{\pm} form). However, in its absence, pair hopping, inter-orbital, and electron-electron intra-orbital interactions render the gap on the electron pockets softly nodal.

PACS numbers: 74.20.Mn, 74.20.Rp, 74.25.Jb, 74.72.Jb

After two years of intense research in the physics of the new iron-based superconductors [1], the symmetry of the order parameter is still far from settled. Theoretically, the current opinion converged on a s_{\pm} nodeless order parameter that changes sign between the electron (e) and hole (h) pockets, which comes out of both the strong and the weak-coupling pictures of the iron-based superconductors [2–6]. However, most of these theories are either phenomenological [7, 8], or use models that take into account only a part of the Fe orbitals present in the material. The most quantitative approaches give anisotropic gaps around the electron Fermi surface which, at their smallest value, are close but do not cross zero [9].

The experimental situation is more controversial. In the 122 compounds, ARPES points to the existence of nodeless isotropic gaps on the hole Fermi surfaces [11, 12]; on the electron Fermi surface, on which ARPES also shows an isotropic gap, the data is less trustful. NMR spin relaxation time shows no coherence peak [13] and exhibits a T^3 power-law right below the transition temperature up to $0.1 - 0.2T_c$, reminiscent of the cuprates nodal behavior. This can be explained by fine-tuning an s_{\pm} order parameter [14]. Penetration depth data on the Fe-As compounds display power-law [15] and exponential [16] behavior. Thermal conductivity shows no residual κ/T intercept, although its in-field dependence points to a large gap anisotropy [17, 18]. By contrast, for LaOFeP, the penetration depth is extremely linear with temperature, and the thermal conductivity shows a large residual intercept, both strong characteristics of nodal superconductivity [19, 20]. This is even more puzzling since both materials have similar Fermi surface topology [21].

In this article, we offer an explanation for the puzzling

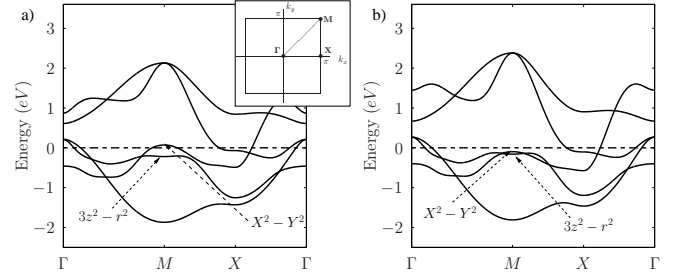


FIG. 1: 2D Band structure for LaOFeAs (a) and LaOFeP (b). (Inset: Brillouin Zone). The tight-binding model for LaOFeAs is contains in-plane hoppings up to fifth nearest-neighbors [5]; the parameters are varied for LaOFeP according to the different pnictogen height parameters given in [10]. The dashed horizontal lines denote the Fermi Level for the undoped compound. The electronic structure looks very similar in both systems. The major difference is the $d_{X^2-Y^2}$ dominated band crossing the Fermi level in (a), but not in (b). Being still away from the Fermi level, the $3z^2 - r^2$ dominated band is shifted up in (b) compared to (a).

difference between the order parameter character in the As and P-based compounds. Using functional renormalization group (fRG) on a 5-band orbital model of the iron-based superconductors with orbital interactions, we find that the gap on the e-pockets can undergo a nodal transition if the third hole pocket at (π, π) is absent. Both ARPES and numerical simulation data show this to be true in the case of LaOFeP [22, 23]. By using an extended orbital model due to Kuroki *et al.* [5, 10], we find that the third h-pocket is overwhelmingly composed of d_{xy} orbital (or $d_{X^2-Y^2}$ in a 45° rotated basis along the Fe-As bonds). When present, the third h-pocket at the (π, π) point in the unfolded Brillouin zone (Fig. 2b)

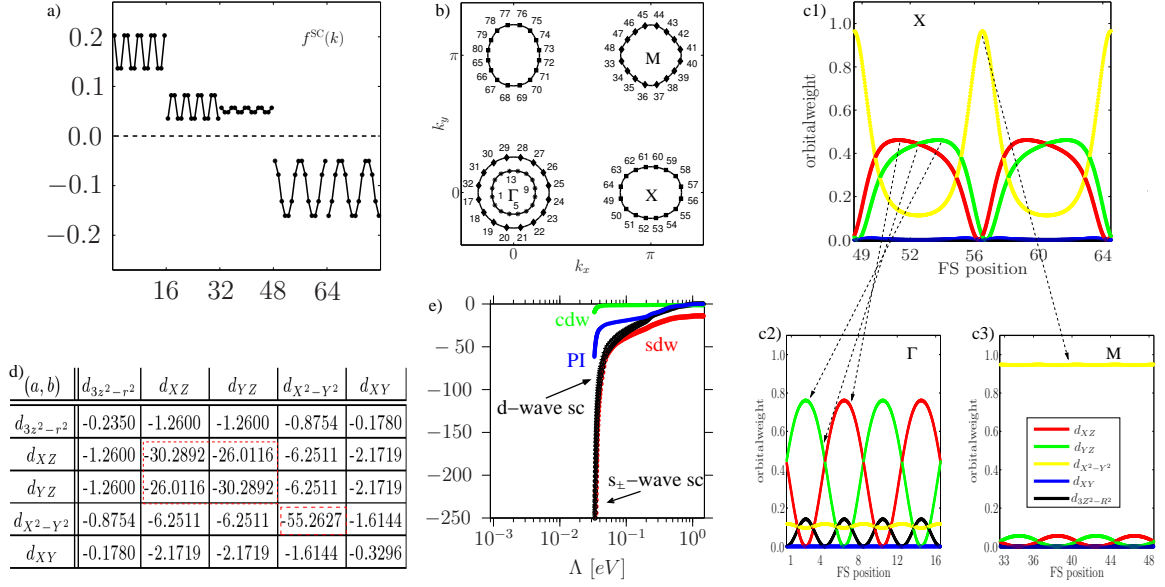


FIG. 2: 5 pocket scenario for As-based compounds. a) Plot of the superconducting form factor gap versus the patching indices (momenta) shown in b). The gap on the outer h-pocket at Γ is smaller than of the inner h-pocket and of the same order as the M pocket gap. The gap on the e-pockets is very anisotropic but nodeless and of opposite sign from h-pocket gap. c1)-c3) Orbital weight distribution on the different pockets (not shown is the outer h-pocket at Γ , which is similar to c2) shifted by 90 degrees assuring orthogonality of the band vectors). Dashed lines indicate most relevant scattering contributions for the dominating U_1 intra-orbital interaction. d) Leading pairing instability eigenvalues $c_{i,(a,b)}^{SC}(\Lambda_c)$ from the orbital decomposition matrix $\langle c_a^\dagger c_a^\dagger \rangle \langle c_b c_b \rangle$ in the Cooper channel. Most relevant weights are on the diagonal and off-diagonal contributions from the $d_{XZ,YZ}$ orbitals as well as the diagonal contribution of $d_{X^2-Y^2}$. e) Flow of leading instability eigenvalues (charge density wave (CDW), Pomeranchuk instability (PI), SDW, and SC). SDW fluctuations are highly relevant, leading (s^\pm); sub-leading (d -wave) SC instabilities as well as SDW diverge in close proximity to each other, where the divergence scale is of $\Lambda_c \approx 0.08\text{eV}$.

scatters through intra-orbital interactions strongly with the d_{xy} part of the e-pockets around the X point to form an s^\pm phase. This enhances the already present s^\pm superconductivity between the Γ point h-pockets and the e-pockets. The gap on the e-pockets is found to be very anisotropic. Upon changing to the P-based structure, the absence of the third h-pocket allows for pair hopping, inter-orbital interactions, and electron-electron (e-e) scattering to drive the already anisotropic gap on the e-pockets nodal. We use a two-dimensional tight-binding model developed by Kuroki *et al.* [5] to describe the band structure of the 1111-type iron-based superconductors:

$$H_0 = \sum_{\mathbf{k},s} \sum_{a,b=1}^5 c_{\mathbf{k}as}^\dagger K_{ab}(\mathbf{k}) c_{\mathbf{k}as}. \quad (1)$$

Here c 's denote electron annihilation operators, and a, b the 5 d Fe orbitals and s the spin indices. While the main electronic structure of P-based and As-based compounds is very similar, there are certain important differences. Fig. 1 shows the band structure of LaOFeAs and LaOFeP, where the latter is obtained by adjusting the parameters in [5] according to the changed pnictogen height from As to P [10]. In the vicinity of the Fermi surface, the most notable difference is the presence or absence of a broad $d_{X^2-Y^2}$ (d_{xy})-dominated band at $M = (\pi, \pi)$, in agree-

ment with ARPES data. To account for this difference, we use a 5 *pocket scenario* for the As-based and a 4 *pocket scenario* for the P-based compounds. We choose to compare and analyze two generic cases, with or without the h-pocket at (π, π) as corresponding to the As-based 1111 (122) and the P-based compounds, respectively.

The interactions in the orbital model are given by:

$$H_{\text{int}} = \sum_i \left[U_1 \sum_a n_{i,a\uparrow} n_{i,a\downarrow} + U_2 \sum_{a < b, s, s'} n_{i,as} n_{i,bs'} + \sum_{a < b} (J_H \sum_{s, s'} c_{ias}^\dagger c_{ibs'}^\dagger c_{ias'} c_{ibs} + J_{\text{pair}} c_{ia\uparrow}^\dagger c_{ia\downarrow}^\dagger c_{ib\downarrow} c_{ib\uparrow}) \right], \quad (2)$$

where $n_{i,as}$ denote density operators at site i of spin s in orbital a . We consider intra- and inter-orbital interactions U_1 and U_2 as well as Hund's coupling J_H and pair hopping J_{pair} . In what follows, we choose a physical interaction setting dominated by intra-orbital coupling, $U_1 > U_2 > J_H \sim J_{\text{pair}}$, and choose $U_1 = 3.5\text{eV}$, $U_2 = 2.0\text{eV}$, $J_H = J_{\text{pair}} = 0.7\text{eV}$ [9]. (Even though the interaction scales are chosen relatively high, the bare effective interaction scale, taking into account different orbital weights, does not exceed $\sim 2\text{eV}$, versus a kinetic bandwidth of $\sim 5\text{eV}$.) This is a rather simplified picture as these scales would in general also depend on

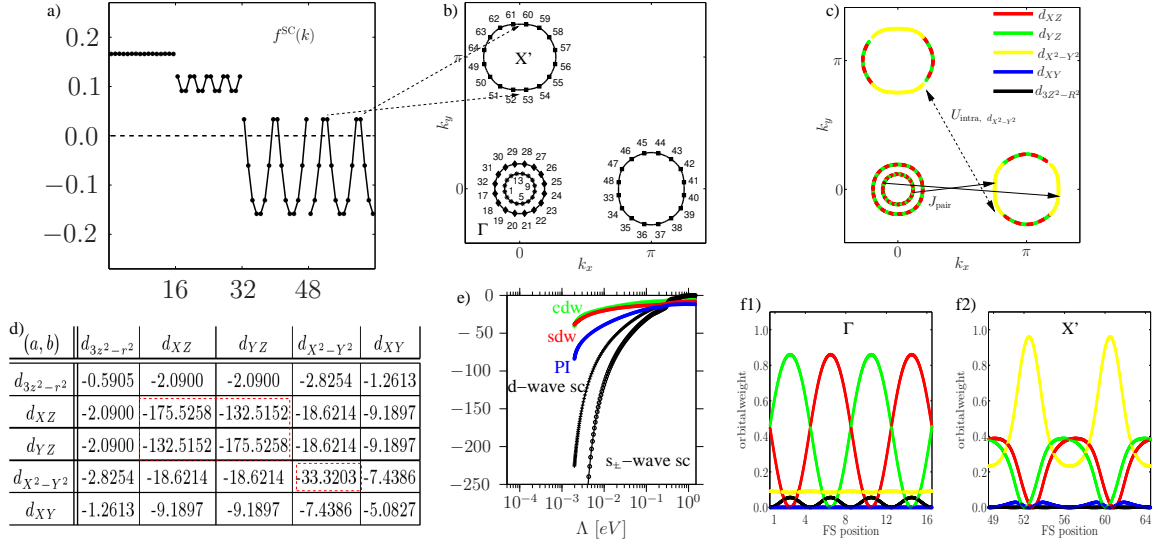


FIG. 3: 4 pocket scenario for LaOFeP. a) Leading s^\pm superconducting form factor gap, with Fermi surface patches given in b); the $d_{X^2-Y^2}$ -dominated h-pocket at M is absent. The h-pockets at Γ are gapped and rather isotropic, with a smaller gap on the outer h-pocket. The e-pockets show a huge anisotropy, being nodal on the inner pockets tips indicated by dashed arrows. c) Important processes leading to nodal channels. Being subleading in the presence of the M hole pocket, J_{pair} scattering processes from the $d_{XZ,YZ}$ dominated Γ pockets to the e-pockets and electron-electron intra-orbital processes between e-pockets now contribute to nodal propensity, with the orbital weight distributions shown in f1)-f2). d) The orbital decomposition matrix of the SC instability show increasing weight on the $d_{XZ,YZ}$ orbitals with a less relevant diagonal $d_{X^2-Y^2}$ contribution. e) Flow of leading instability eigenvalues (notation as in Fig. 2e); nodal s^\pm is favored; the SDW fluctuations are comparably weak. The divergence scale $\Lambda_c \approx 0.0065\text{eV}$ is much less than for the As-based materials.

the different orbitals. However, for the two scenarios representative for As- and P-based compounds, we checked that the main features are stable under variation of these parameters. From the band structure point of view, it should also be noted that the $d_{3z^2-r^2}$ -dominated band moves towards the Fermi level for the P-based compound (Fig. 1). However, this band only plays a marginal role since no other relevant band has this orbital content and hence any scattering to other bands would be governed by sub-leading inter-orbital interactions. We defer a refined discussion to a later stage [24]. Using functional renormalization group (fRG) [9, 25–28], we study how the renormalized interaction described by the 4-point function (4PF) evolves under integrating high energy fermionic modes; the flow parameter is the IR cutoff Λ approaching the Fermi surface, i.e. $V_\Lambda(\mathbf{k}_1, n_1; \mathbf{k}_2, n_2; \mathbf{k}_3, n_3; \mathbf{k}_4, n_4) c_{\mathbf{k}_4 n_4 s}^\dagger c_{\mathbf{k}_3 n_3 \bar{s}}^\dagger c_{\mathbf{k}_2 n_2 s} c_{\mathbf{k}_1 n_1 \bar{s}}$, with \mathbf{k}_1 to \mathbf{k}_4 the incoming and outgoing momenta. Due to the spin rotational invariance of interactions, we constrain ourselves to the $S^z = 0$ subspace of incoming momenta $\mathbf{k}_1, \mathbf{k}_2$ (and outgoing $\mathbf{k}_3, \mathbf{k}_4$) and generate the singlet and triplet channel by symmetrization and antisymmetrization of the 4PF V_Λ [27]. The starting conditions are given by the kinetic bandwidth serving as an UV cutoff, with the bare initial interactions for the 4PF. The diverging channels of the 4PF under the flow to the Fermi surface signal the nature of the instability, and Λ_c serves as an upper bound for the transition

temperature T_c . For a given instability characterized by some order parameter $\hat{O}_{\mathbf{k}}$ (the most important example of which is the SC instability $\hat{O}_{\mathbf{k}}^{\text{SC}} = c_{\mathbf{k}} c_{-\mathbf{k}}$ in our case), the 4PF in the particular ordering channel can be written as $\sum_{\mathbf{k}, \mathbf{p}} V_\Lambda(\mathbf{k}, \mathbf{p}) [\hat{O}_{\mathbf{k}}^\dagger \hat{O}_{\mathbf{p}}]$ [29]. Accordingly, the 4PF in the Cooper channel can be decomposed into different eigenmode contributions

$$V_\Lambda^{\text{SC}}(\mathbf{k}, -\mathbf{k}, \mathbf{p}) = \sum_i c_i^{\text{SC}}(\Lambda) f^{\text{SC}, i}(\mathbf{k})^* f^{\text{SC}, i}(\mathbf{p}), \quad (3)$$

where i is a symmetry decomposition index, and the leading instability of that channel corresponds to an eigenvalue $c_i^{\text{SC}}(\Lambda)$ first diverging under the flow of Λ . $f^{\text{SC}, i}(\mathbf{k})$ is the SC form factor of pairing mode i which tells us about the SC pairing symmetry and hence gap structure associated with it. In fRG, from the final Cooper channel 4PFs, this quantity is computed along the discretized Fermi surfaces, and the leading instability form factors are plotted in Fig. 2a and 3a.

As-based compounds: For the As-based setting, we find that the s^\pm instability is the leading instability of the model at moderate doping. The setup resembles the situation studied in [9], which, as an additional check, we also studied with a more detailed tight-binding structure beyond 5th next-nearest neighbors. We likewise find a nodeless s^\pm SC leading instability. However, we can identify the M h-pocket to play a major role in contributing to the SDW fluctuations and to support the full gapping

of the s -wave as well as sign-change from hole to electron pockets (Fig. 2). In particular, we study the orbital content in detail and analyze how the pairing instability distributes over the different orbitals (Fig. 2d). For this, we consider the 4PF in orbital space,

$$V_{c,d \rightarrow a,b}^{\text{orb}} = \sum_{n_1, \dots, n_4=1}^5 \left\{ V_{\Lambda}(\mathbf{k}_1, n_1; \mathbf{k}_2, n_2; \mathbf{k}_3, n_3; \mathbf{k}_4, n_4) \right. \\ \left. \times u_{an_1}^*(\mathbf{k}_1) u_{bn_2}^*(\mathbf{k}_2) u_{cn_3}(\mathbf{k}_3) u_{dn_4}(\mathbf{k}_4) \right\}, \quad (4)$$

where the u 's denote the different orbital components of the band vectors. The matrix shown in Fig. 2d gives the leading eigenvalue contributions of $V_{\Lambda, (a,b)}^{\text{SC}}(\mathbf{k}, \mathbf{p}) = \langle c_{\mathbf{k},a}^{\dagger} c_{-\mathbf{k},a}^{\dagger} \rangle \langle c_{\mathbf{p},b} c_{-\mathbf{p},b} \rangle$, in the Cooper channel of (4). As in (3), we decompose it into different form factor contributions $\sum_i c_{i,(a,b)}^{\text{SC}}(\Lambda) f_{(a,b)}^{i,\text{SC}}(\mathbf{k})^* f_{(a,b)}^{i,\text{SC}}(\mathbf{p})$, where the leading eigenvalues at Λ_c for different (a,b) are plotted in Fig. 2d and 3d. We observe a leading contribution in the diagonal part of the $d_{X^2-Y^2}$ orbital, which is strongly linked to the scattering contributions from the M h-pocket to the $d_{X^2-Y^2}$ -dominated parts of the e-pockets (Fig. 2). The main scattering processes are intra-orbital scattering between the d_{xz} (or d_{yz}) orbitals-dominated parts of the e- and Γ h-pockets. These processes favor an s^{\pm} SC instability, as was found in [9]. However, there is another process in the case of As-based superconductors: Along the $\Gamma \leftrightarrow X$ path, the e-pocket has a high concentration of the $d_{X^2-Y^2}$ orbital. This part of the e-pocket then scatters strongly with the 3rd h-pocket at the M -point, which is entirely made of the $d_{X^2-Y^2}$ orbital band. The intra-orbital repulsion on them prefers an s^{\pm} -type pairing between the M h-pocket and the e-pocket, which reinforces the already present s^{\pm} between the Γ h-pockets and the X (X') e-pockets. With the commonly-used assumption that U_{intra} is the dominant interaction, it then seems likely that the 3 h-pockets display a gap of identical sign: the two Γ -pockets, which are not nested with each other and hence can have the same gap sign and are of different orbital content than the M h-pocket. This then allows all these gaps to have the same sign. However, the e-pockets contain contributions from all 3 mainly relevant d orbitals, and therefore scatter strongly through U_{intra} with all 3 h-pockets, which enhances the s^{\pm} character of the gap. The presence of the 3rd hole pocket is also responsible for the strong SDW signal, being due to the fact that the nesting wave-vector $M \leftrightarrow X$ is the same as $\Gamma \leftrightarrow X$. Below we will indeed see below that the absence of this pocket weakens the SDW.

P-based compounds: Moving to the P-based compound case changes the physical picture even qualitatively. As shown in Fig. 3, we find a nodal s^{\pm} scenario for the P-based compounds, with lower critical divergence scale $\Lambda_c \sim T_c$ and less SDW-type fluctuations. The *absence of SDW order* in the P-based compounds is a well-known experimental fact. Here, the absence of the M hole pocket

removes the intra-orbital scattering contribution to the electron pockets. This gives way to previously subleading scattering channels like e-e scattering between the $d_{X^2-Y^2}$ -dominated parts of the e-pockets and pair hopping from the h-pockets at Γ to the e-pockets. They tend to drive this part of the e-pockets nodal (Fig. 3c). As another check, we applied constant band interactions to the As-based and P-based setups to analyze the pure Fermi surface topology unaffected by orbital-specific interaction effects. This means that we do not take into account the orbital content at a Fermi surface point, but choose a general set of couplings g that is only specified by the type of intra- or inter-pocket scattering [25, 26]. We find that the intensity of $(0, \pi)$, $(\pi, 0)$ SDW fluctuations is indeed strongly influenced by the scattering contributions $M \leftrightarrow X$. Constant band interactions show very isotropic gaps on the e-pockets [25, 26]. As a consequence, the electron gap anisotropy, rendering the electron gap nodeless or nodal, is a phenomenon of orbital interactions, in accordance with above elaborations. Furthermore, we varied the intra-orbital interaction scale on the $d_{X^2-Y^2}$ orbital and the J_{pair} scale in the P-based scenario. Increasing these scales, it triggers the propensity to form nodes on the electron pockets. Furthermore, under this variation, the electron pocket part of the form factor can be considerably shifted to being more or less nodal.

These tendencies all appear to be consistent with experiment: we find (i) a lower divergence scale and hence lower critical temperature, (ii) significantly enhanced low energy density of states in the superconducting phase, and (iii) reduced SDW type fluctuations, which, even at pronounced nesting, are insufficient to drive the system to a leading magnetic SDW instability [19–21]. The absence of the hole pocket at M also manifests itself in the orbital decomposition of the pairing instability Fig. 3d: The diagonal contribution of $d_{X^2-Y^2}$, in comparison to the $d_{XZ,YZ}$, is significantly reduced.

We find that the relevance of the broad band at the unfolded M point plays the major role to explain the drastic change of properties from the As-based to the P-based 1111 compounds, rendering the former nodeless and the latter nodal. The nodes that appear in the P-based compounds are driven by anisotropy and are not given by any new SC pairing symmetry, which remains of s^{\pm} type. A more detailed work on the technical background and broader scope of this work is in progress [30].

We thank C. Honerkamp, J. Hu, K. Kuroki, D.-H. Lee, Z. Tesanovic, A. Vishwanath, and F. Wang for discussions. RT is supported by a Feodor Lynen Fellowship of the Humboldt Foundation. RT, CP, and WH are supported by DFG-SPP 1458/1. BAB acknowledges support from the Alfred P. Sloan Foundation and Princeton University startup funds.

-
- [1] Y. Kamihara, T. Watanabe, M. Hirano, and H. Hosono, *J. Am. Chem. Soc.* **130**, 3296 (2008).
 - [2] K. Seo, B. A. Bernevig, and J. Hu, *Phys. Rev. Lett.* **101**, 206404 (2008).
 - [3] I. I. Mazin, D. J. Singh, M. D. Johannes, and M. H. Du, *Phys. Rev. Lett.* **101**, 057003 (2008).
 - [4] S. Graser, T. A. Maier, P. J. Hirschfeld, and D. J. Scalapino, *New Journal of Physics* **11**, 025016 (2009).
 - [5] K. Kuroki *et al.*, *Phys. Rev. Lett.* **101**, 087004 (2008).
 - [6] V. Stanev, J. Kang, and Z. Tesanovic, *Phys. Rev. B* **78**, 184509 (2008).
 - [7] M. M. Korshunov and I. Eremin, *Phys. Rev. B* **78**, 140509 (2008).
 - [8] A. V. Chubukov, D. V. Efremov, and I. Eremin, *Phys. Rev. B* **78**, 134512 (2008).
 - [9] F. Wang, H. Zhai, Y. Ran, A. Vishwanath, and D.-H. Lee, *Phys. Rev. Lett.* **102**, 1047005 (2009).
 - [10] K. Kuroki, H. Usui, S. Onari, R. Arita, and H. Aoki, *Phys. Rev. B* **79**, 224511 (2009).
 - [11] L. Wray *et al.*, *Phys. Rev. B* **78**, 184508 (2008).
 - [12] H. Ding *et al.*, *Eur. Phys. Lett.* **83**, 47001 (2008).
 - [13] K. Matano *et al.*, *Eur. Phys. Lett.* **83**, 57001 (2008).
 - [14] M. M. Parish, J. Hu, and B. A. Bernevig, *Phys. Rev. B* **78**, 144514 (2008).
 - [15] K. Hashimoto *et al.*, *Phys. Rev. Lett.* **102**, 207001 (2009).
 - [16] L. Malone *et al.*, *Phys. Rev. B* **79**, 140501 (2009).
 - [17] M. A. Tanatar *et al.*, arXiv:0907.1276.
 - [18] J. G. Checkelsky *et al.*, arXiv:0811.4668.
 - [19] M. Yamashita *et al.*, *Phys. Rev. B* **80**, 220509 (2009).
 - [20] C. W. Hicks *et al.*, *Phys. Rev. Lett.* **103**, 127003 (2009).
 - [21] D. H. Lu *et al.*, *Physica C* **469**, 452 (2009).
 - [22] D. H. Lu *et al.*, *Nature* **455**, (2008).
 - [23] A. Carrington *et al.*, *Physica C* **469**, 459 (2009).
 - [24] C. Platt, R. Thomale, B. A. Bernevig, and W. Hanke, in preparation.
 - [25] C. Platt, C. Honerkamp, and W. Hanke, *New J. Phys.* **11**, 055058 (2009).
 - [26] R. Thomale, C. Platt, J. Hu, C. Honerkamp, and B. A. Bernevig, *Phys. Rev. B* **80**, 180505 (2009).
 - [27] C. Honerkamp, M. Salmhofer, N. Furukawa, and T. M. Rice, *Phys. Rev. B* **63**, 035109 (2001).
 - [28] R. Shankar, *Rev. Mod. Phys.* **66**, 129 (1994).
 - [29] H. Zhai, F. Wang, and D.-H. Lee, *Phys. Rev. B* **80**, 064517 (2009).
 - [30] R. Thomale *et al.*, in preparation.